# Mid-infrared laser-induced superheating of water and its quantification by an optical temperature probe

Tobias Brendel and Ralf Brinkmann

Free-running thulium laser pulses (Cr:Tm:YAG, $\lambda = 2.01$ μm, $t_p = 300$ μs) were applied to a purified, degassed water sample and the resulting temperature rise was investigated by an optical temperature probe. The probe detected water reflectance index changes with temperature and also the onset of vaporization, which was found to occur in a superheat regime, at approximately 230 °C. The experimental data were compared with theoretical temperature calculations, and deviations of less than 20 °C were stated. The best agreement between theory and experiment was found for temperatures below 180 °C, defining by this the method's high accuracy limit. In conclusion, both the optical temperature probe and the presented calculations can help to improve dosimetry in pulsed IR laser applications by precise temperature measurement and prediction. 

*OCIS codes:* 170.0170, 170.1020, 350.5340, 300.1030, 120.1880, 000.6850.

## 1. Introduction

The 2-μm wavelength is of major interest for numerous medical laser applications. It combines a relatively high absorption in tissue with the property to be transmittable through optical silica fibers. The latter enables easy handling of the radiation and its use in endoscopic applications.[1] Moreover, because of the high absorption the tissue can be ablated precisely, since the energy deposition is confined to a small volume. The most common laser systems that emit at the 2-μm wavelength are the thulium laser (Cr:Tm:YAG, $\lambda = 2.01$ μm) and the holmium laser (CTH:YAG, $\lambda = 2.09$ and 2.12 μm).

The tissue ablation is based on the vaporization of tissue water, which is the main absorbent for 2-μm radiation. Secondary effects accompany the ablation, such as thermal denaturation and tissue tearing that is due to thermoelastic stress. All these damage mechanisms have in common that their appearance and effect strongly depend on temperature. Consequently, a reliable dosimetry is coupled to a precise knowledge of the temperatures achieved in the tissue. This again implies the need for precise data for temperature-dependent absorption coefficients. For this reason we recently published accurately measured data for the 2-μm water absorption at the thulium and holmium laser wavelengths.[2] The measurements were performed at ambient pressure and over a temperature range between 20 and 100 °C. As a result, a linear dependency $\mu(T) = a + bT$ of negative slope $b$ was found at both laser wavelengths. On the basis of these results, any laser-induced temperature rise within the (20 . . . 100 °C) interval can be calculated from the applied radiant exposure. For radiant exposures that induce higher temperatures the calculations can proceed in a first-order approximation by linear extrapolation of the given functions $\mu(T)$.

Brinkmann and Hansen[3] and Frenz *et al.*[4] demonstrated that pulsed thulium and holmium laser irradiation of water can generate transient temperatures far above the normal boiling point. The reasons for this behavior are complex, going back to nucleation conditions and the influence of thermoelastic pressure transients.

It is our aim to quantify the actual superheat being generated when thulium laser pulses are applied to a water sample. To this end we adapted the optical temperature probe proposed by Hooper *et al.*[5] and measured exemplarily the temperature rise after applying free-running thulium laser pulses. The experimental results were compared with temperature calculations on the basis of the linearly extrapolated function $\mu(T) = a + bT$. These calculations were

T. Brendel (brendel@scimedia.de) is at Brunnenstrasse 15/8, 55120 Mainz, Germany. R. Brinkmann (brinkmann@mll.muluebeck.de) is with the Medical Laser Center Luebeck, Peter-Monnik-Weg 4, 23562 Luebeck, Germany.

Received 12 July 2003; revised manuscript received 1 December 2003; accepted 8 December 2003.

0003-6935/04/091856-07$15.00/0

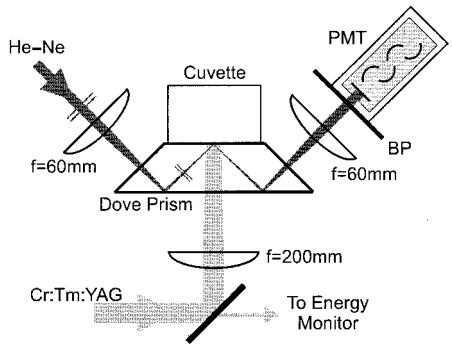

Fig. 1. Experimental setup.

further improved by also taking into consideration the temperature dependence of the density and specific heat.

## 2. Experimental Methods

The experiments were performed with a free-running Cr:Tm:YAG laser ($\lambda = 2.01$ μm, pulse duration $t_p = 300$ μs) with a pure $TEM_{00}$ mode profile (beam quality $M^2 \approx 1.2$). The laser radiation was guided through a fused-silica dove prism (Almaz Optics, Marlton, N.J., substrate KU-1) into a cuvette that contained a sample of purified, degassed water (Fig. 1). To achieve sufficiently high radiant exposures, the laser beam diameter was reduced by an $f = 200$-mm focusing lens, yielding a $(1/e^2)$ beam radius $w = 257 \pm 3$ μm at the immersed prism wall. The depth of focus (Rayleigh length) was 1.5 mm, giving a quasi-parallel beam over the optical penetration depth of $\delta \approx 150$ μm in the water sample. Radius $w$ was precisely determined by a standard knife-edge technique.[6] Given pulse energy $E$, the radiant exposure $H$ (mJ/mm$^2$) at the center of the thulium beam was calculated according to $H = 2E/(\pi w^2)$. This value was taken for the temperature calculations.

### A. Optical Temperature Probe

The optical temperature probe basically consists of an immersed glass prism and a He–Ne laser beam that is directed to the glass–water interface (Fig. 1). With this arrangement changes in temperature are detected by corresponding reflectance changes that are due to the temperature dependence of the water refractive index $n_W(T)$. For our experiments a $p$-polarized, Gaussian He–Ne probe beam was coupled into the dove prism as shown in Fig. 1 to be incident at approximately 45° to the silica–water interface. By means of an $f = 60$-mm focusing lens we focused the beam to a radius of approximately 8 μm. The lens was mounted on a three-dimensional micropositioner to be axially and laterally alterable. By axial altering, the focus of the probe beam was located on the silica–water interface. Moving the lens laterally, we placed the focus at the center of the thulium laser beam. Both adjustments were performed under control of a CCD camera that took images of the immersed prism surface through a glass window in the opposite cuvette wall. After recollimation by a second lens, the reflected part of the probe beam was detected by a photomultiplier tube (PMT). The PMT was protected from ambient light by a narrowband He–Ne bandpass filter (BP) ($\Delta\lambda \pm 0.2$ nm).

It should be noted that we focused the probe beam for two reasons: First, to attain a sufficient spatial resolution for temperature probing in the center of the thulium laser beam, and second, to ensure a single incident angle of the probe beam to the silica–water interface. This is due to the wave-optical fact that the wave front in the waist of a Gaussian beam is plane.

Given incident angle $\alpha$, the relation between reflectance $R_\parallel$ and water refractive index $n_W(T)$ is expressed by the Fresnel relation

$$R_\parallel(T)|_\alpha = \left\{\frac{\tan[\alpha - \beta(T)]}{\tan[\alpha + \beta(T)]}\right\}^2, \tag{1}$$

in common with Snellius's law

$$\beta(T) = \arcsin\left[\frac{n_P \sin(\alpha)}{n_W(T)}\right]. \tag{2}$$

Here, $R_\parallel$ denotes the reflectance of the $p$-polarized probe beam being incident on the prism–water interface as shown in Fig. 1. Further, $n_P = 1.457$ indicates the refractive index of the prism substrate (fused silica, $T = 20$ °C, $\lambda = 633$ nm). It can be represented by a constant because its changes with temperature[7] are negligible compared with those of $n_W(T)$ (see Section 4).

### B. Calibration

Measured reflectance $R_\parallel$ can be converted to a corresponding temperature on the basis of Eq. (1), $R_\parallel(T)|_\alpha$. Near the $\alpha = 45°$ incident angle, the reflectance rises fast with temperature, which is advantageous for the sensitivity of the probe. On the other hand, the reflectance also responds sensitively to changes in incident angle. Hence, the exact value of $\alpha$ has to be determined in a preliminary calibration measurement.

For this purpose, a heater rod was attached to the cuvette to heat the water sample continuously from 20 to 95 °C. During this time, the intensity of the reflected probe beam was measured in steps of 5 °C. Then all the intensities were normalized to the 20 °C value to convert them to relative reflectances. The resulting data are shown in Fig. 2. Here, the horizontal error of ±2 °C reproduces the precision of the thermocouple that we used. The vertical error of ±0.04 originates from signal noise. Now we numerically fitted the theoretical course $[R_\parallel(T)/R_\parallel(20\ °C)]_\alpha$ to the data by varying the incident angle. As a best fit, $\alpha = 44.2 \pm 0.1°$ was found (see Fig. 2). This value was confirmed when we performed a second calibration procedure after the IR laser experiments were completed.

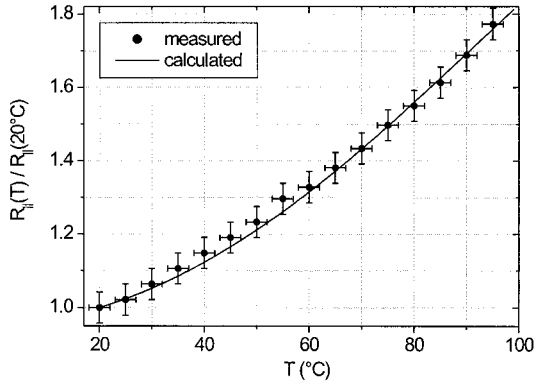


Fig. 2. Calibration measurement to determine incident angle α. The solid curve shows the theoretical course $[R_\parallel(T)/R_\parallel(20\ °C)]_\alpha$ for the best-fit angle $\alpha = 44.2°$.

### C. Detection of Vaporization Onset

Because there are different refractive indices for water ($n_W \simeq 1.3$ at 633 nm) and vapor ($n_V \simeq 1$), the onset of vaporization causes a pronounced reflectance rise and can therefore be detected by the optical temperature probe as well. For this application, the probe's sensitivity took considerable advantage of the $\alpha = 44.2°$ incident angle, which can be explained as follows: Without vaporization α is close to the Brewster angle $\alpha_B = 42.4°$ of the silica–water interface and so the reflectance for the *p*-polarized probe light is correspondingly low. If vaporization starts, α exceeds the critical angle $\alpha_{crit} = 43.3°$ of the silica–vapor interface such that the probe light is totally reflected. Altogether, this provides a reflectance rise of 4 orders in magnitude.[6]

## 3. Calculation of Laser-Induced Temperature Rise

In a first approach heat diffusion can be neglected such that the temperature increase $\partial T$ that is due to absorption of the applied irradiance $I(t)$ (W/mm$^2$) is given by

$$\partial T = \epsilon(T) I(t) \partial t,$$

where

$$\epsilon(T) = \frac{\mu(T)}{\rho(T) C(T)}. \tag{3}$$

Here, μ is the absorption coefficient at the regarded laser wavelength, ρ is the density of liquid water, and $C$ is the heat capacity, which is either $C_p$ in the case of an isobaric temperature change (slow heating by long laser pulses) or $C_V$ if the irradiation takes place under stress confinement conditions (fast heating by short laser pulses).

The temperature dependence of variable ϵ turns Eq. (3) into a differential expression of a linear differential equation. To solve Eq. (3), the temperature dependencies of all the parameters, μ, ρ, and $C$, were merged to a single polynomial fit $\epsilon(T) = a + bT + cT^2$. The coefficients were determined for all the combinations of irradiation cases, i.e., for all the combinations of $\mu_{Ho}$, $\mu_{Tm}$, $C_p$, and $C_V$ (see Table 1). The fits of $(\mu/\rho C)(T)$ were based on the linear functions $\mu_{Tm,Ho}(T)$ as published previously,[2] and on data for ρ and $C_{p,V}$ from two sources. For temperatures $T \in (20 \ldots 100\ °C)$, the data were taken from the industrial standard IAPWS-97,[8] and for temperatures $T \in [100 \ldots 240\ °C]$ from the work of Skripov.[9] Note that all the data relate to ambient pressure $p = 1$ bar.

With the second-order polynomial representation of $\epsilon(T)$, Eq. (3) can be integrated analytically,[10] yielding

$$T(H) = \frac{b - \gamma - (b + \gamma) f(T_0) \exp(H\gamma)}{2c[f(T_0)\exp(H\gamma) - 1]}, \tag{4}$$

where $\gamma = \sqrt{b^2 - 4ac}$, $T_0$ is the ambient temperature, and

$$f(T_0) = \frac{2cT_0 + b - \gamma}{2cT_0 + b + \gamma}. \tag{5}$$

Here, $H(t) = \int_{-\infty}^{t} I(\tau)\mathrm{d}\tau$ (mJ/mm$^2$) denotes the radiant exposure being applied up to the time $t$. For this paper all the temperatures are meant to be end temperatures ($t \to \infty$) calculated from $H = \int_{-\infty}^{\infty} I(\tau)\mathrm{d}\tau$. The solution in Eq. (4) implies that $b^2 - 4ac > 0$ is fulfilled, which was fulfilled for all the regression coefficients listed in Table 1.

### A. Influence of Heat Diffusion (into the Prism Substrate)

The axial temperature profile in the water sample initially follows the Lambert–Beer absorption law with the maximum temperature rise being located right at the prism wall. As time progresses, heat diffusion into the prism body reduces the temperature rise at the prism wall and causes the maximum temperature rise to move deeper into the water. Additionally, heat diffusion within the liquid rehomogenizes the axial temperature profile and reduces, in particular, the maximum temperature rise. Radial heat diffusion, on the other hand, can be neglected for the pulse duration and beam radius.

**Table 1. Coefficients of the Polynomial Regression[a]**

| Coefficient | $\mu_{Tm}/\rho C_p$ | $\mu_{Tm}/\rho C_V$ | $\mu_{Ho}/\rho C_p$ | $\mu_{Ho}/\rho C_V$ |
|---|---|---|---|---|
| $a$ (°C mm$^2$/mJ) | 6.840 | 6.65 | 3.318 | 3.253 |
| $b$ (mm$^2$/mJ) | −0.02207 | −0.0119 | $-8.49 \times 10^{-3}$ | $-4.4 \times 10^{-3}$ |
| $c$ (mm$^2$/°C mJ) | $1.27 \times 10^{-5}$ | $-4.3 \times 10^{-5}$ | $-5.7 \times 10^{-6}$ | $-1.2 \times 10^{-5}$ |
| Maximum deviation | <0.1% | <0.1% | <0.4% | <2% |

[a] $(\mu_{Ho,Tm}/\rho C_{p,V})(T) = a + bT + cT^2$; see text for more details.

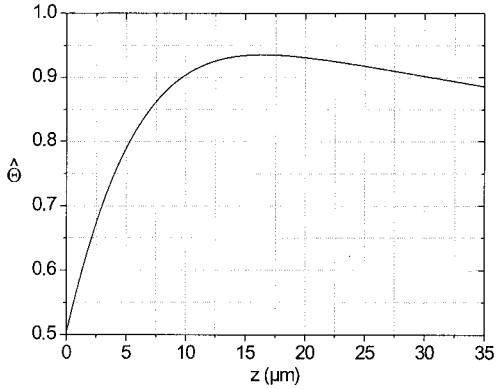


Fig. 3. Axial profile of the normalized temperature rise $\hat{\Theta}(z) = \Theta(z)/\Theta_0$ at the end of a 300-μs laser pulse (solid curve). The prism wall is located at $z = 0$.

To quantify the axial heat diffusion we refer to the work of Hooper *et al.*[5] who presented an analytical solution for this problem. It is based on a one-dimensional heat equation that considers heat flow into the prism body. The laser energy is assumed to be deposited instantaneously, yielding an initial temperature distribution $\Theta(z) = \Theta_0 \exp(-\mu z)$, with $\Theta \equiv T - T_0$. Consequently, the given solution of $\Theta_\delta(z, t)$ has the character of an impulse response, which is indicated by the δ subscript. We then calculated the temperature rise $\Theta(z, t)$ to a temporally extended irradiation by convolving the impulse response with the temporal power profile $I(t)$ of the laser pulse:

$$\Theta(z, t) = [\Theta_\delta(\tau, z) \otimes I(\tau)](t) = \int_{-\infty}^{\infty} \Theta_\delta(t - \tau, z) I(\tau) \mathrm{d}\tau. \quad (6)$$

If, for simplicity, the pulse profile is assumed to be rectangular with duration $t_p$, Eq. (6) reduces to

$$\Theta(z, t_p) = \frac{1}{t_p} \int_0^{t_p} \Theta_\delta(\tau, z) \mathrm{d}\tau. \quad (7)$$

Computing Eq. (7) for the experimental pulse duration $t_p = 300$ μs one obtains a temperature profile as depicted in Fig. 3. In this graph the profile is normalized to the initial maximum temperature rise $\Theta_0$ such that the absolute temperature changes to any radiant exposure $H$ can be read off easily by calculating $T(H) - T_0$ according to Eq. (4) and multiplying this value with the normalized profile $\hat{\Theta}(z) = \Theta(z)/\Theta_0$.

With respect to the optical temperature probe, the axial temperature profile reveals that the measured temperature rise at the prism wall ($z = 0$) amounts to only 55% of the maximum temperature rise at $z \approx 17$ μm. Moreover, this maximum amounts to only 93% of the $\Theta_0$ value being attained without heat diffusion (instantaneous energy deposition). Correspondingly, to compare the experimental results with the temperature calculations $T(H)$ according to Eq. (4), two corrections must be made. The experimental data obtained with the temperature probe at the prism wall must be corrected by a factor of $1/0.55 \simeq 1.82$, whereas the calculated temperature rise $\Theta(H) = T(H) - T_0$ must be corrected by a factor of 0.93.

### 4. Temperature Dependence of Water Refractive Index

The water refractive index is not only a function of temperature but of density as well. At constant pressure, the density itself is solely a function of temperature, such that the concatenation $n_W(T)|_p = n_W[T, \rho(T)|_p]$ yields the wanted relation between temperature and refractive index. The liquid pressure remains constant during irradiation if the acoustic transit time $\tau_{ac}$ through the heated volume is shorter than the pulse duration $t_p$, i.e., if the condition of stress confinement is not fulfilled.[11] Given the speed of sound $c = 1480$ m/s in water, the proximate dimensions of the heated volume by beam radius $w$, and the optical penetration depth $\delta = 1/\mu$, the acoustic transit time can be expressed as $\tau_{ac} = \min(w, \delta)/c$. With the radiation parameters used ($w = 257$ μm, $\delta = 150$ μm) one can obtain $\tau_{ac} \approx 120$ ns, which differs by 3 orders of magnitude from the overall pulse duration $t_p = 300$ μs and still by 1 order of magnitude by the mean spike duration $t_s = 1.5$ μs within the laser pulse profile (see Fig. 4). Hence, temperature probing can be assumed to take place at ambient pressure.

As mentioned above, the function $\rho(T)|_p$ is known at ambient pressure to a superheat of 240 °C. The water refractive index $n_W(T, \rho)$ was thoroughly studied by Schiebener *et al.*[12] They gave an implicit polynomial representation for the $\rho$–$T$ dependencies of $n_W$ being valid for temperatures $T \in (-10 \ldots 500$ °C), densities $\rho \in (0 \ldots 1045$ kg/m$^3$), and wavelengths $\lambda \in (200 \ldots 2500$ nm). These ranges cover all the experimentally expected values for $\rho$ and $T$ and also contain wavelength $\lambda = 633$ nm of the He–Ne probe beam. By a simple transformation the implicit representation is turned into the desired form $n_W(T, \rho)$. The resulting temperature course $n_W(T) \equiv n_W[T, \rho(T)|_p]$ at $p = 1$ bar is plotted in Fig. 5. It can be expressed with high accuracy by the following polynomial ($\lambda = 633$ nm):

$$n_W(T) = n_{W,0} + n_{W,1} T + n_{W,2} T^2, \quad (8)$$

where

$$n_{W,0} = 1.33438 \pm 1 \times 10^{-5},$$
$$n_{W,1} = -8.715 \times 10^{-5} \pm 4 \times 10^{-8} (1/°\mathrm{C}),$$
$$n_{W,2} = -8.159 \times 10^{-7} \pm 4 \times 10^{-10} (1/(°\mathrm{C})^2).$$

### 5. Results and Discussion

#### A. Onset of Vaporization

In Fig. 4 two typical power profiles of the free-running thulium laser are plotted along with the intensity traces that were simultaneously recorded by the PMT. Both graphs illustrate the strict correspondence between the stepwise intensity rise and the spikes of the power profile, also stepwise raising

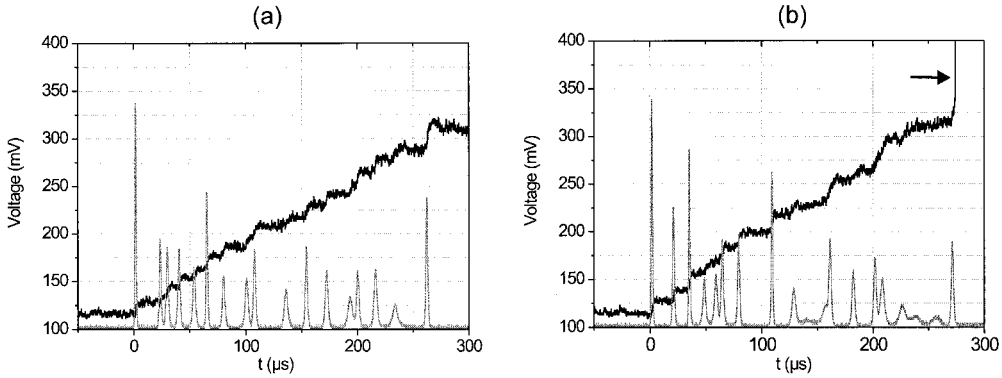


Fig. 4. (a) Intensity rise as measured by the PMT (mV) during irradiation with a free-running thulium laser pulse of indicated power profile [gray line, (a.u.)] and a total radiant exposure $H = 277$ mJ/mm$^2$. The same in (b) for another pulse of similar radiant exposure $H = 279$ mJ/mm$^2$. Note the pronounced signal rise at the end of this pulse (marked by an arrow), indicating the onset of vaporization.

the temperature in the water sample. In contrast to these moderate signal changes, a strong signal rise is visible at the end of the right signal trace, which indicates the onset of vaporization by total reflection of the probe light at the formation of the glass–vapor interface. To quantify the threshold radiant exposure for the vaporization onset we applied and correlated a series of $N = 120$ laser pulses with varying pulse energy to the number of vaporization events. In this way, we found the vaporization probality as a function of radiant exposure.[6] A characteristic value of this function is the $ED_{50}$ radiant exposure, belonging to a vaporization probability of 50%. It was determined to be $ED_{50} \simeq 300$ mJ/mm$^2$ and defined to be the threshold radiant exposure for the vaporization onset in our experiment.

### B. Temperature Probing to Vaporization

The optical temperature probe was used with laser pulse applications of radiant exposures below or equal to the $ED_{50}$ value for vaporization onset. With the aim to determine the maximum water temperature, the reflected probe light intensities $I_{\mathrm{end}}$ (mV) at the end of the laser pulses were recorded and evaluated as follows: First, they were converted into relative reflectance changes by normalizing them to intensity $I(20\ ^\circ\mathrm{C})$ being measured before pulse application. Second, the inverse of the calibration curve $[R_\parallel(T)/R_\parallel(20\ ^\circ\mathrm{C})]_\alpha$ (see Fig. 2) was computed and the laser-induced temperature rises $T(H) - T_0$ were read off from the measured reflectance changes. Third, according to the heat diffusion model described above, the maximum temperature rise in the water sample was achieved by multiplying the evaluated temperature rises at the prism wall by a factor of 1.82. Finally, the ambient temperature $T_0 = 20\ ^\circ\mathrm{C}$ was added to obtain absolute temperatures. The results are summarized in Fig. 6. In addition, two calculated temperature courses $T(H)$ are plotted in this graph. The solid curve represents $T(H)$ according to Eq. (4). The dotted curve is based on a calculation for which only the temperature dependence of the absorption was considered, whereas density ρ and specific heat $C_p$ were assumed to be constant. In other words, the dotted curve represents the previous way of calculating $T(H)$.[3] All the calculations consider heat diffusion by means of the above-described

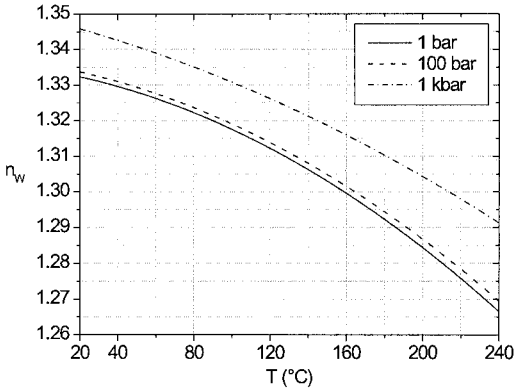


Fig. 5. Temperature dependence of the water refractive index $n_W$ ($\lambda = 633$ nm) at ambient pressure and, for comparison, at $p = 100$ bar and $p = 1$ kbar (see text for more details).

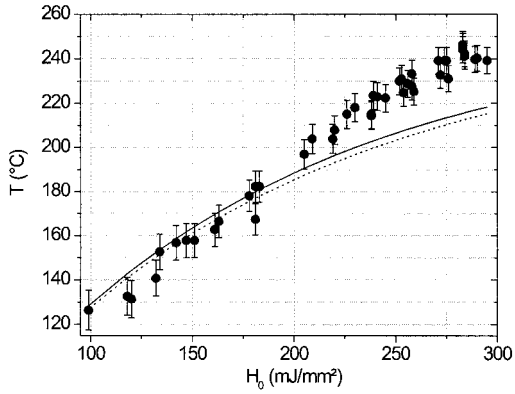


Fig. 6. Maximum water temperature as evaluated from data of the optical temperature probe at the prism wall (single spots) and according to temperature calculations $T(H)$ (solid and dotted curves). The vertical error bars in the experimental data reflect uncertainties in the temperature determination that are due to signal noise (visible in the traces of Fig. 4).

correction factor of 0.93 for the calculated maximum temperature rise $\Theta(H) = T(H) - T_0$.

In comparison, the two ways of calculating $T(H)$ differ so little (<3 °C) that the temperature dependencies of $\rho$ and $C_p$ seem to be negligible versus $\mu(T)$. This in fact is the main reason for the observed similarity, since the relative change of the absorption amounts to 82% over the regarded temperature range, whereas $\rho$ and specific heat $C_p$ change by only 18% and 14%, respectively. Moreover, these changes are counteracting, i.e., $\rho$ decreases, while $C_p$ increases, such that the product $\rho \cdot C_p$ remains practically constant. This differs if the specific heat at constant volume is used to describe a process that takes place in the stress confinement regime. There $C_V$ decreases with temperature (by −24%) and so the decrease of $\rho$ is further enhanced. As a result, the previous and the present way of calculating $T(H)$ differ in this case by 20 °C (at $H = 300$ mJ/mm$^2$), which must be rated as significant.

By comparing the calculated temperatures with the experimental data we found good agreement in the lower temperature range. Yet, for temperatures above 180 °C, the calculations systematically underestimate the experimental values. This observation is most likely explained by a progressive deviation of the real absorption course $\mu(T)$ from the linear extrapolation in such a manner that the linear extrapolation lowers the absorption too rapidly. Consequently, the calculations deliver too low temperatures for a given radiant exposure. On the other hand, several assumptions in the underlying heat diffusion model also rate the experimental data's accuracy carefully. As described above, the heat diffusion model connects the calculated maximum temperature rise to that being measured at the prism wall. Here, the temperature dependencies of the water and silica thermal diffusivities and conductivities were neglected as well as the actual power profile of the laser pulses.

Still, both the measurements and the calculations indicate that the onset of vaporization was related to a water temperature of approximately 230 °C. Hence, a pronounced superheat was realized in the particular water sample. When Frenz *et al.*[4] applied pulsed holimum laser radiation to a distilled water sample, they claimed to have generated temperatures of up to 280 °C, the highest water superheat being experimentally realized so far.[13] However, this temperature was calculated assuming a constant absorption. Considering its temperature dependence, a superheat of only 200 °C was found, which is in the range of our results.

### C. Influence of Stress Transients on Temperature Probe

Using $Q$-switched IR laser pulses, the pulse durations reduce typically to some tens or hundreds of nanoseconds. On these time scales, stress confinement is possible and thermoelastic stress transients of significant amplitude can develop. Since the water refractive index $n_W$ is also a function of pressure, these stress transients can perturb the optical temperature probe as long as they are present at the prism wall. To quantify this effect, Fig. 5 shows the function $n_W(T)$ at ambient pressure and at $p = 100$ bar and 1 kbar for comparison. The three curves illustrate that the refractive index falls with temperature but rises with pressure. Consequently, a thermoelastic pressure rise can reduce or even compensate the changes of $n_W$ with temperature. For example, if heating the sample from 20 °C to 90 °C is accompanied by a stress generation of 1 kbar, $n_W$ is of the same size as with room temperature and $p = 1$ bar. Hence, when we use the optical temperature probe with $Q$-switched laser pulses, a temporary disfunction of the probe during the presence of acoustic transients must be taken into account.

## 6. Conclusions

Free-running thulium laser pulses were applied to a purified, degassed water sample and the consequent temperature rise was investigated by an optical temperature probe. Two main results were found: First, the water superheat was determined to be approximately 230 °C, thus remaining clearly below the ultimate limit of 280 °C. Second, the presented temperature calculations were confirmed up to a temperature of approximately 180 °C. The measurement accuracy was limited mainly by signal noise, yielding error bars in the region of ±10 °C. With the regression polynomial $n_W(T)|_p$ being derived for $p = 1$ bar and $T \in (20\ °C \ldots 240\ °C)$ in this study, the optical temperature probe becomes adaptable to any experimental setup. As a result, the dosimetry in pulsed IR laser applications can now be supported by direct temperature measurements or by precise temperature prediction on the basis of evaluated equations.

The authors thank the FAZIT-Stiftung, Frankfurt am Main, Germany, for supporting this research.

## References

1. R. Brinkmann, D. Theisen, T. Brendel, and R. Birngruber, "Single-pulse 30-J holmium laser for myocardial revascularization: a study on ablation dynamics in comparison to $CO_2$ laser-TMR," IEEE J. Sel. Top. Quantum Electron. **5,** 969–980 (1999).
2. B. I. Lange, T. Brendel, and G. Hüttmann, "Temperature dependence of light absorption in water at holmium and thulium laser wavelengths," Appl. Opt. **41,** 5797–5803 (2002).
3. R. Brinkmann and C. Hansen, "Beam-profile modulation of thulium laser radiation applied with multimode fibers and its effect on the threshold fluence to vaporize water," Appl. Opt. **39,** 3361–3370 (2000).
4. M. Frenz, F. Könz, H. Pratisto, and H. P. Weber, "Starting mechanisms and dynamics of bubble formation induced by a Ho:Yttrium aluminum garnet laser in water," J. Appl. Phys. **84,** 5905–5912 (1998).
5. B. A. Hooper, Y. Domankevitz, R. R. Anderson, and C. Lin, "Optical temperature probe," Appl. Phys. Lett. **78,** 2381–2383 (2001).
6. T. Brendel and R. Brinkmann, "Highly resolved tracing of Q-switched mid-IR laser-induced vaporization," in *Laser–Tissue Interaction XII: Photochemical, Photothermal, and Photomechanical*, D. D. Duncan, S. L. Jacques, and P. C. Johnson, eds., Proc. SPIE **4257,** 303–311 (2001).

7. I. H. Malitson, "Interspecimen comparison of the refractive index of fused silica," J. Opt. Soc. Am. **55,** 1205–1209 (1965).
8. "Release on the IAPWS Industrial Formulation 1997 for the Thermodynamic Properties of Water and Steam," available at http://www.iapws.org.
9. V. P. Skripov, *Thermophysical Properties of Liquids in the Metastable* (*Superheated*) *State* (Gordon & Breach, New York, 1988).
10. I. N. Bronstein and K. A. Semendjajew, *Taschenbuch der Mathematik* (Nauka, Moscow, 1991).
11. M. Frenz, G. Paltauf, and H. Schmidt-Kloiber, "Laser-generated cavitation in absorbing liquid induced by acoustic diffraction," Phys. Rev. Lett. **76,** 3546–3549 (1996).
12. P. Schiebener, J. Straub, J. M. H. Levelt Sengers, and J. S. Gallagher, "Refractive index of water and steam as function of wavelength, temperature and density," J. Phys. Chem. Ref. Data **19,** 677–717 (1990).
13. P. G. Debenedetti, *Metastable Liquids: Concepts and Principles* (Princeton University, Princeton, N.J., 1996).